

SEISMIC SOURCE AND LOCAL SITE EFFECTS ON LONG-PERIOD GROUND MOTIONS FROM THE 2003 TOKACHI-OKI EARTHQUAKE

T. Maeda¹ and T. Sasatani²

¹ *Researcher, Faculty of Science, Hokkaido University, Sapporo, Japan*

² *Professor, Graduate School of Engineering, Hokkaido University, Sapporo, Japan*

Email: tmaeda@mail.sci.hokudai.ac.jp

ABSTRACT :

We study characteristics of long-period ground motions from the 2003 Tokachi-oki earthquake (Mj 8.0), a large interplate earthquake, based on spatial distribution maps and attenuation relationships of PGV (peak ground velocity) value for four period ranges; wide band and three narrow bands (central periods of 10, 20, and 30 s). The spatial distribution maps for all kinds of PGV value show azimuth dependence; the PGV values in northern side of the epicenter are larger than those in southwestern side of the epicenter, when compared at a comparable distance. These features result from the radiation pattern of long-period surface waves; that is, the source effect. The attenuation relationships indicate that the PGV values for the wide-band period range are affected by ground motions with periods less than 10 s at distances less than 200 km, while long-period surface waves mainly contribute to them at distances larger than 200 km. The basin site effects generate a patchy pattern in the spatial distribution maps and a large scattering in the attenuation relationships of PGV values for the wide-band and 10 s period ranges. We examine the site effect of the Sarobetsu basin located at the northern tip of Hokkaido based on the observation data and simulations. Finally we conclude that the PGV values from the 2003 Tokachi-oki earthquake are controlled by the radiation pattern of long-period S and surface waves, and various basin site effects.

KEYWORDS: the 2003 Tokachi-oki earthquake, long-period ground motion, spatial distribution of PGV, attenuation relationship of PGV

1. INTRODUCTION

On 26 September 2003 JST (25 September UTC), the Tokachi-oki earthquake (Mj 8.0; magnitude after Japan Meteorological Agency, JMA) occurred at the south off Hokkaido, Japan (Fig. 1). During the earthquake, long-period ground motion damaged huge oil tanks due to a sloshing phenomenon at Tomakomai about 200 km away from the epicenter (Hatayama et al. 2004; Koketsu et al. 2005). Damage to high-rise and large-scale structures due to long-period ground motion has been observed during past large earthquakes (e.g., the 1964 Niigata and 1983 Nihonkai-chubu earthquakes in Japan and the 1985 Michoacan earthquake in Mexico). We have re-realized from the 2003 Tokachi-oki earthquake that long-period ground motion has potential to cause serious damage to high-rise and large-scale structures even at a long distance.

The 2003 Tokachi-oki earthquake is a large interplate earthquake between the Pacific and Okhotsk plates, where large interplate earthquakes periodically occur. At the south off Hokkaido, a previous large earthquake (Mj 8.2) with almost the same epicenter as the 2003 Tokachi-oki earthquake occurred in 1952 (Fig. 1). The 1952 Tokachi-oki earthquake was recorded at several JMA stations. Maeda and Sasatani (2004) compared JMA strong motion (displacement) seismograms from the 1952 and 2003 Tokachi-oki earthquakes at several stations. They pointed out that the waveforms from the two events are mutually similar at each station, and that the peak amplitudes at Wakkanai and Sendai differ by up to 10 times, even though they locate at a comparable epicentral distance (Fig. 1). This fact motivated us to study a spatial distribution of long-period ground motions from the 2003 Tokachi-oki earthquake.

The 2003 Tokachi-oki earthquake is the first M 8 class earthquake in Japan since dense strong-motion networks (e.g., K-NET and KiK-net) have been deployed all over Japan. The numerous strong motion data from this

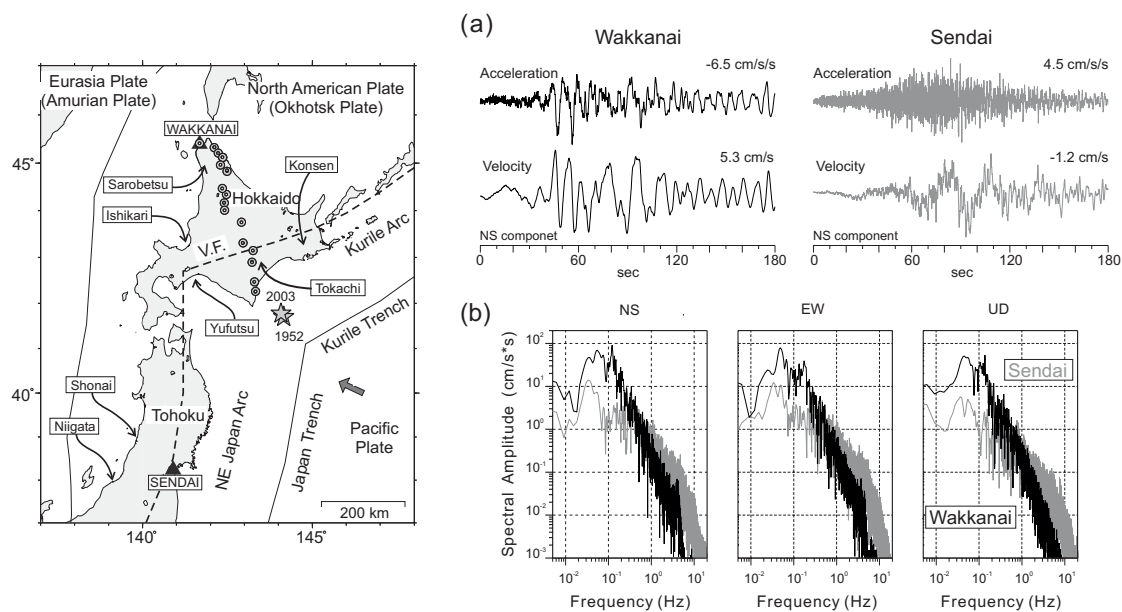


Figure 1. Left: A location map showing tectonic setting in the eastern Japan. Stars show epicenters of the 1952 and 2003 Tokachi-oki earthquakes determined by JMA. Solid triangles are JMA stations, Wakkanai and Sendai. V.F. indicates the volcanic front. Location of large sedimentary basins is also shown. Gray circles are stations used in the waveform simulation (Fig. 2). Right: A comparison of strong motion records from the 2003 Tokachi-oki earthquake observed at Wakkanai and Sendai. (a) Acceleration and velocity seismograms (N-S component). (b) Velocity Fourier spectra of three-component records. Black and gray lines represent the data for Wakkanai and Sendai, respectively.

earthquake provide a good opportunity for studying seismic source, propagation path and site effects on strong ground motion over the wide period range. In this paper, we first show a preliminary study of long-period ground motions from the 2003 Tokachi-oki earthquake to illustrate the regional-scale characteristics. Then, we examine the spatial distribution map and attenuation relationship of peak ground velocity (PGV) using the K-NET, KiK-net and JMA strong motion data (the total number of stations used is 755) and derive the seismic source and site effects on long-period ground motion. Finally we examine the site effect of the Sarobetsu basin located at the northern tip of Hokkaido based on the observation data and simulations. A part of this study was published in Maeda and Sasatani (2008).

1.1 Preliminary Study of Strong Ground Motion

First we examine characteristics of strong ground motion from the 2003 Tokachi-oki earthquake based on data at Wakkanai and Sendai. Figure 1(right, a) shows acceleration and velocity seismograms at the two stations. On the accelerograms, short-period waves predominate at Sendai but strongly attenuate at Wakkanai. This is due to heterogeneous Q_s (quality factor for S wave) structure beneath Hokkaido and Tohoku; that is, propagation path effect (e.g., Maeda and Sasatani, 2006; Morikawa et al., 2006). On the other hand, long-period waves with periods of 10 to 30 s predominate on the velocity seismograms; however, the peak amplitude at Wakkanai is about five times larger than that at Sendai. A particle motion diagram of these long-period waves shows that Rayleigh wave dominates at Wakkanai and Love wave dominates at Sendai. The characteristics of the long-period surface waves depend on epicenter-to-station azimuth.

Figure 1(right, b) shows velocity Fourier spectra (time window is about 120 s) at the stations. The spectral shapes differ between the stations. The Wakkanai spectra have larger spectral amplitudes than the Sendai spectra for frequencies below 0.5 Hz, while the Sendai spectra have larger amplitudes than the Wakkanai spectra for frequencies over 0.5 Hz. The velocity spectral amplitudes at Wakkanai have a peak at around 0.05

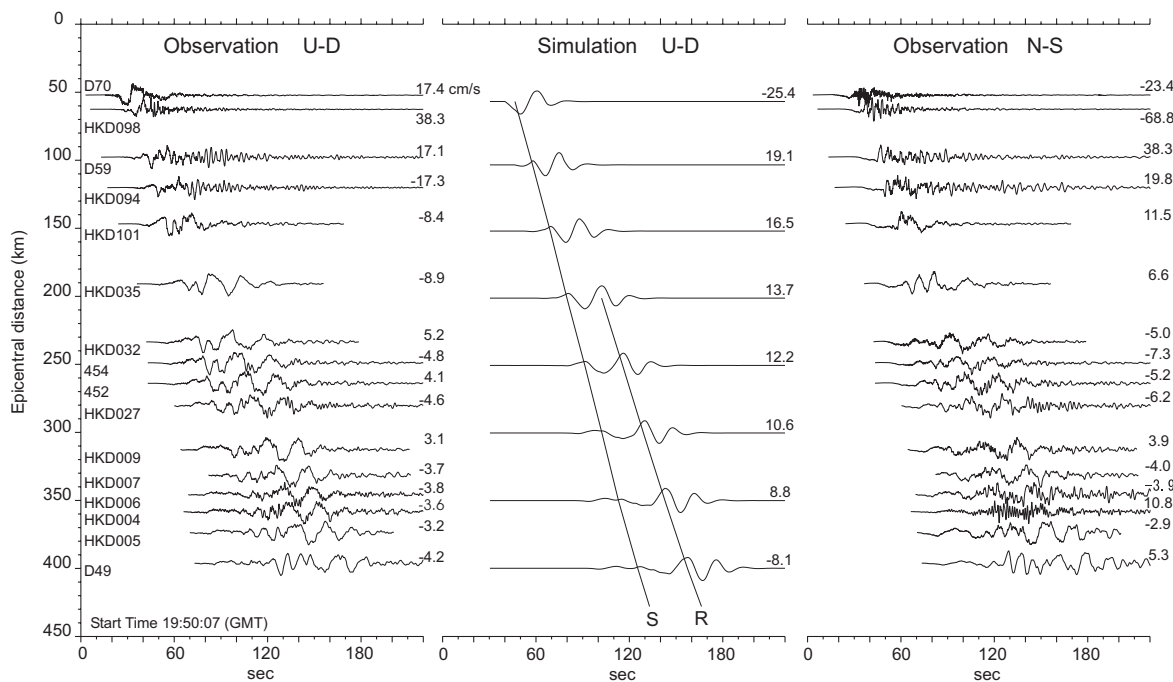


Figure 2. Velocity seismograms (U-D and N-S components) along the N340°E profile. The simulated U-D component seismograms are also shown in the central column. In this figure, an S-wave travel time curve is shown with a phase velocity of Rayleigh wave. A location of the profile is shown in Fig. 1 left.

Table I. Velocity structure used in the waveform simulation.

	Vp (km/s)	Vs (km/s)	Density (g/cm ³)	Thickness (km)	Qp	Qs
1	6.0	3.5	2.7	10.0	600	300
2	6.4	3.7	2.8	20.0	600	300
3	8.0	4.5	3.3		1000	500

Hz and 0.1 Hz; those at Sendai have a peak at around 0.03 Hz. The velocity seismograms and their spectra indicate that the long-period waves contribute to PGV values for the 2003 Tokachi-oki earthquake.

Next we examine velocity waveforms as a function of distance. Figure 2 shows velocity seismograms (U-D and N-S components) at stations along the N340°E profile; the profile is shown in Fig. 1. Simulated waveforms (U-D components) and an S-wave travel-time curve along the same profile are also shown for the sake of interpretation of the observed waveforms; the simulation method is mentioned in the next section. The comparison between the observed and simulated waveforms shows that long-period S waves contribute to PGV at stations with distances less than about 150 km, while long-period surface waves (Rayleigh waves) contribute to PGV at stations with distances larger than about 200 km. The N-S component seismograms are rather rich in short-period waves and have larger amplitudes compared with the U-D component ones. The short-period waves, however, are riding on a long-period carrier, thus the long-period waves play the primary role in contributing to PGV.

From above preliminary studies, we concluded to examine characteristics of long-period ground motion from the 2003 Tokachi-oki earthquake based on PGV values not only for original velocity seismograms but also for band-pass filtered velocity seismograms.

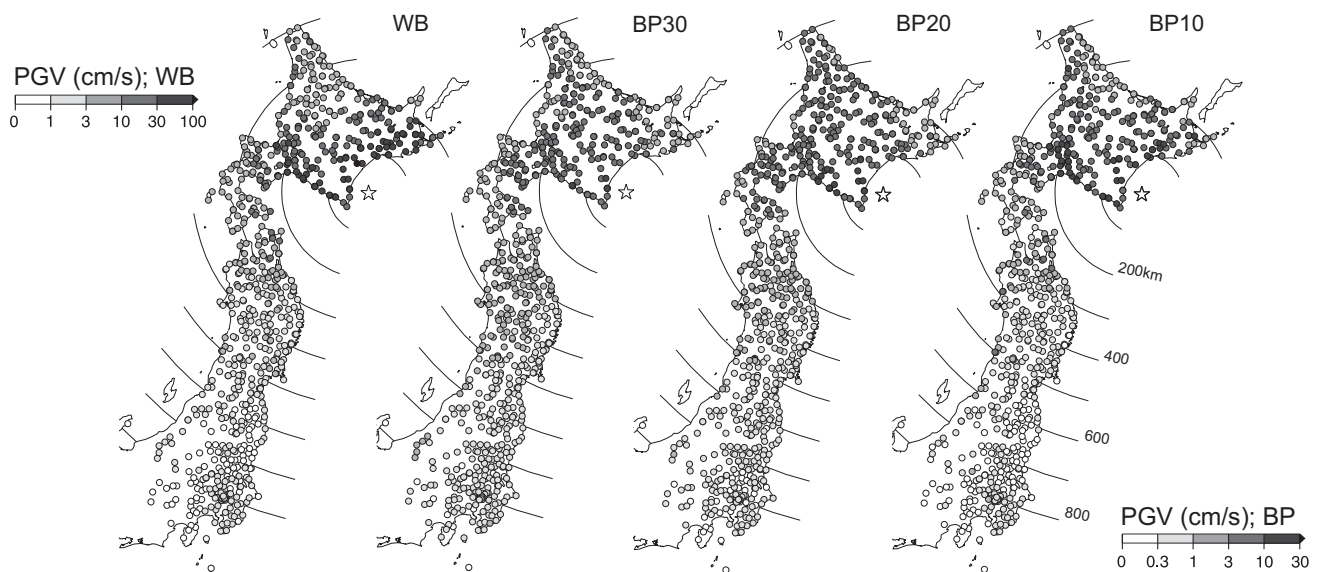


Figure 3. Spatial distribution maps of the four kinds of PGV (peak ground velocity) value from the 2003 Tokachi-oki earthquake. WB: PGV value from wide-band velocity seismograms. BP10, BP20 and BP30: PGV value from band-pass filtered velocity seismograms with a central period of 10, 20 and 30 s, respectively. An open star is a centroid epicenter determined by Harvard University. Concentric circles indicate distances from the hypocenter. Note that the color scale is different between the WB and BP data.

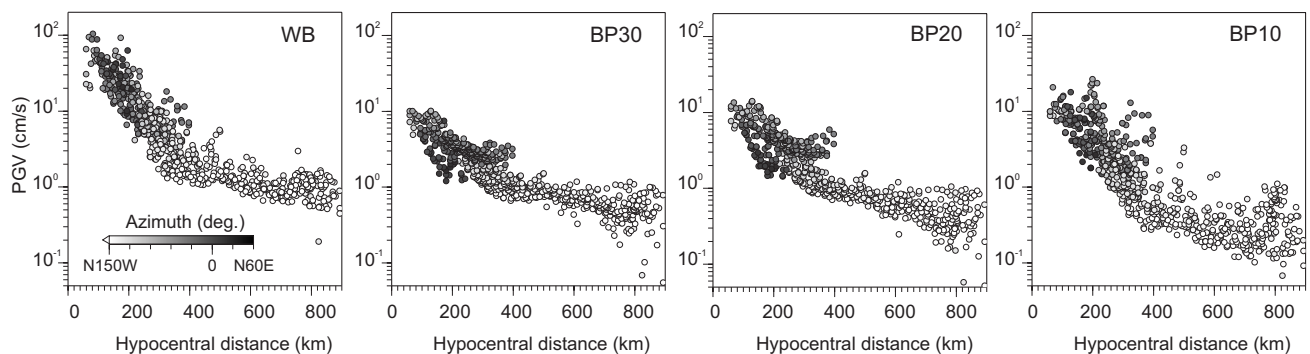


Figure 4. Attenuation relationships of the four kinds of PGV (peak ground velocity) value from the 2003 Tokachi-oki earthquake. Color scale indicates epicenter-to-station azimuth.

2. SPATIAL DISTRIBUTION AND ATTENUATION RELATIONSHIP OF PGV VALUES

We make four kinds of velocity seismogram after integration of the original accelerogram. The first kind is a wide-band velocity seismogram that is obtained by high-pass filtering with a cut-off frequency of 0.01 Hz. The other three kinds are narrow band-pass filtered velocity seismograms with different central frequencies; the central frequencies (periods) used are 0.1 Hz (10 s), 0.05 Hz (20 s) and 0.033 Hz (30 s). PGA value is a maximal value of vector sum of the three-component velocity seismograms. The four kinds of PGV value taken from the four kinds of velocity seismogram are abbreviated as PGV(WB), PGV(BP10), PGV(BP20) and PGV(BP30), respectively.

Figure 3 shows spatial distribution maps of the four kinds of PGV value. At first glance, all kinds of PGV value show a regional-scale distribution pattern that the PGV values in Hokkaido, northern side of the epicenter, are larger than those in Tohoku, southwestern side of the epicenter, when compared at a comparable distance. It is

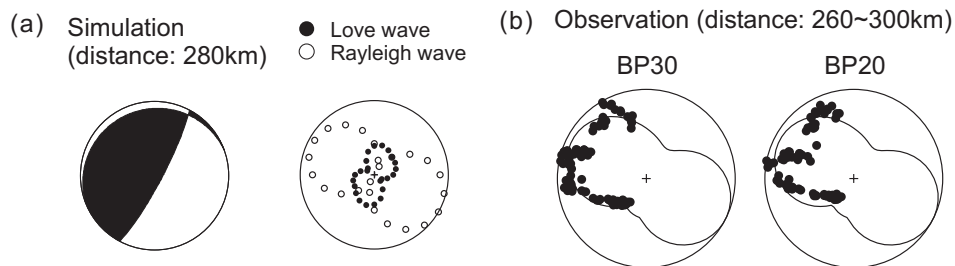


Figure 5. (a) Left: Focal mechanism of the 2003 Tokachi-oki earthquake determined by Harvard University. Right: Radiation pattern of Rayleigh (open circles) and Love (solid circles) waves at a hypocentral distance of 280 km; these are taken from simulated velocity seismograms. (b) A comparison of the observed and simulated radiation patterns around a distance of 280 km. Solid circles are observed values and a curved line, simulated ones, respectively.

well known that PGA (peak ground acceleration) values on the fore-arc side of the volcanic front are much larger than those on the back-arc side of the volcanic front (e.g., Morikawa et al., 2006); this regional-scale distribution pattern is generated by the path effect of anomalous upper mantle structure beneath island arc (e.g., Maeda and Sasatani, 2006). However, such distribution pattern is not recognized in any kinds of PGV value. This suggests that the peculiar pattern for PGV values is not due to the path effect but due to the source effect. Further, several sites have the larger PGV values compared with the surrounding sites. For example, stations on the Yufutsu, Ishikari, Tokachi, Konsen and Sarobetsu basins in Hokkaido, and the Shonai and Niigata basins in Tohoku, have the larger PGV values, especially in the PGV(WB) and PGV(BP10) maps; locations of these basins are shown in Fig. 1. This patchy pattern is due to the site effect of large sedimentary basins.

Attenuation relationships for the four kinds of PGV value are shown in Fig. 4. We simply take a centroid epicenter (42.20° , 143.84°) by Harvard University and a focal depth of 40km, which corresponds to a plate boundary depth at the epicenter, as an origin of the hypocentral distance. In interpretation of the attenuation relationships, we should note that the azimuthal coverage of the data points changes with the distance range. In addition, the characteristics of long-period surface waves depend on epicenter-to-station azimuth as shown in the previous section. Therefore, we classify the data points according to the azimuth.

Figure 4 shows following trends. At distance (D) less than 200 km, the PGV(WB) values are larger than the sum of the PGV(BP30), PGV(BP20) and PGV(BP10). This indicates that the PGV(WB) values in this distance range are affected by ground motions with periods shorter than 10 s. At $200 < D < 300$ km, the sum of the PGV(BP30), PGV(BP20) and PGV(BP10) are comparable to the PGV(WB) values. At $D > 300$ km, the PGV(BP30) and PGV(BP20) mainly contribute to the PGV(WB) values. Furthermore the decay rate of the attenuation relationships becomes gentle around a distance of 300 km. Considering the observed waveforms shown in Fig. 2, these trends indicate that S waves mainly contribute to the PGV(WB) values at distances less than 200 km, while long-period surface waves mainly contribute to the PGV(WB) values at distances larger than 200 km.

The attenuation relationships for the PGV(WB) and PGV(BP10) show a large scattering by one order at the distance ranges of $150 < D < 240$ km, $320 < D < 400$ km, $D \sim 500$ km and 600 km; the large scattering results from upward protruding points. These distance ranges include stations on large sedimentary basins as mentioned above (Figs. 1 and 3). The site effect at these basins is considered as a main factor in the large scattering of the PGV(BP10) attenuation relationship. However, the data points at $240 < D < 300$ km also show a scattering by a factor of three to five, though these points are taken from stations out of large sedimentary basins (see Fig. 3). In addition, the PGV(BP30) and PGV(BP20) in this distance range clearly show azimuthal dependence; stations in the north to west range have larger values compared with those in the south-west range.

We examine a main factor in the scattering at $D \sim 280$ km for the PGV(BP30) and PGV(BP20) based on the waveform simulation. For this distance, observed data are taken from stations over the wide-azimuth range. In

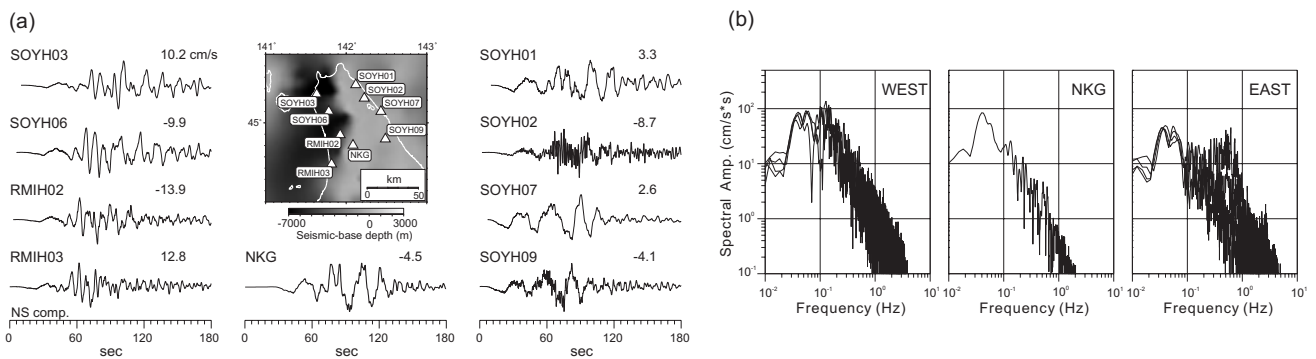


Figure 6. Velocity seismograms (a) and Fourier spectra (N-S component) (b) observed at nine stations in the northern Hokkaido. An inset map shows the station locations and depths of upper boundary of V_s 3.2 km/s layer, where V_s is S-wave velocity.

the simulation we use the discrete wavenumber method (Bouchon, 1981; Takeo, 1985) assuming a one-dimensional stratified structure (Table 1). We refer to the centroid moment tensor solution by Harvard University for the focal mechanism ((strike, dip, rake) = (250°, 11°, 132°); Fig. 5a left), seismic moment ($M_0=3.05 \times 10^{21}$ Nm; M_w 8.3) and epicenter. The focal depth of the centroid moment tensor solution is 28 km, but here we set it to be 40 km. A simple moment rate function (a bell-shaped pulse) having pulse width of 20 s is used. One of simulated results is shown in Fig. 2 for the U-D component.

Figure 5a right shows simulated azimuthal distribution of peak velocity amplitudes for Rayleigh waves and Love waves at a hypocentral distance of 280 km. In this figure, we take a peak amplitude of simulated particle motion on the vertical-radial plane as the Rayleigh wave value and that of the simulated transverse component as the Love wave value. This figure indicates that Rayleigh waves predominate over the wide-azimuth range except the NNE-SSW direction. Figure 5b shows the comparison of azimuthal distributions of the PGV values between the observation and simulation at $D \sim 280$ km. Observation data are taken from stations located within the hypocentral distances from 260 to 300 km. The simulated waveforms have about two times larger amplitudes than the observed ones (see Fig. 2), but here we discuss only the radiation pattern. The data points are plotted using amplitudes normalized by the maximum value for each case. Although the observed PGV values show some scattering, the general patterns agree with the simulated ones. Hence, the PGV scattering at $D \sim 280$ km for the PGV(BP30) and PGV(BP20) is explained by the radiation pattern of the long-period surface waves; that is, the source effect. The attenuation relationships for the PGV(BP30) and PGV(BP20) show large scattering due to azimuthal dependence at the distance range of 100–200 km. This may be caused by the radiation pattern of long-period S wave. We should note that the rupture propagation can produce directivity effect on the radiation pattern. However, it is somewhat difficult to decide that the radiation pattern including the directivity effect more reasonably fits the observed data, because there are no data in the south-eastern side of the epicenter.

3. SITE EFFECTS ON LONG-PERIOD GROUND MOTION

In the previous section, we have recognized several basins, where the site effects on long-period ground motion have been observed, from the spatial distribution map and attenuation relationship for the PGV(BP10); the locations are shown in Fig. 1. The site effect studies of these basins except the Sarobetsu basin have been done by several authors (e.g., Hatayama et al., 2004; Yoshida and Sasatani, 2005). Here we examine the site effect of the Sarobetsu basin located at the northern tip of Hokkaido (Fig. 1).

Figure 6 shows observed velocity seismograms (N-S component) and their Fourier spectra (time window is about 180 s) at nine stations in the northern Hokkaido. Station locations together with depth distribution of seismic basement (Suzuki et al., 2004) are shown in the inset map; the western side of the region with the deep

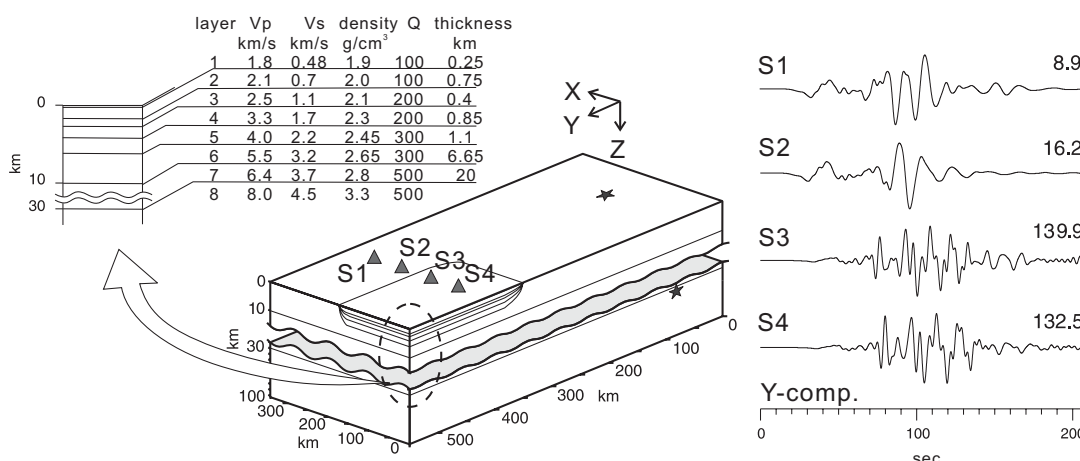


Figure 7. Left; underground structure model used in the waveform simulation. Stars show a projection of the hypocenter on surface and vertical section. Triangles are stations for calculating waveforms. Right; simulated velocity waveforms at stations S1~S4; S1 and S2 are located on a basin. The waveforms are normalized.

basement corresponds to the Sarobetsu basin. Many stations are located on Holocene deposits, but the NKG station of F-net is located in observational vault, that is, a rock site; so the site effects are ignorable. On the seismograms at NKG and the eastern stations, the 20-s period waves predominate; these are Rayleigh waves propagated from the epicenter as shown in Fig. 2. On the other hand, about 10-s period waves dominate on the seismograms at the western stations; the Wakkanai velocity seismogram shown in Fig. 1 has the same nature as mentioned earlier. The amplitudes at the western stations are much larger than those at NKG and the eastern stations except the SOYH02 station, where short-period waves (1.7s) predominate. The Fourier spectra show a clear difference in amplitudes at about 0.1 Hz; the amplitudes at the western stations are several times larger than those at NKG and the eastern stations. From above considerations it is certain that the 20-s period Rayleigh waves at the eastern stations are incident waves into the northern Hokkaido, and that the 10-s period waves at the western stations are basin-transduced surface waves (Kawase and Sato, 1992; Kawase, 1993). This is the site effect of the Sarobetsu basin during the 2003 Tokachi-oki earthquake.

The site effect of the Sarobetsu basin is examined based on a waveform simulation. Simulation is performed by a 3D finite-difference method using discontinuous grids (Aoi and Fujiwara, 1999) for a 3D underground structure model. We simply model the Sarobetsu basin as shown in Fig. 7 and calculate velocity waveforms at four stations in and out of the basin. A grid spacing for a shallow region (<10km) is fine (0.5km), while that for a deep region is three times coarser (1.5km). A double couple point source (see Fig.5) located at 40 km depth is used; its source time function is a Ricker wavelet with a characteristic period of 20 s; source time function is different from that used in the discrete wavenumber method (Fig. 2).

The calculated waveforms at basin sites (S3, S4) contain much short-period waves and have larger amplitudes compared with those at rock sites (S1, S2) (Fig. 7). These features are similar to the observation (Fig. 6b). The dominant period of the short-period waves at the basin sites (about 6 s) is slightly shorter than that of the observations (about 10 s). This discrepancy may come from the simplicity of the assumed structure model. Modification of the structure model will give a good agreement of the dominant period, but that is not the purpose of this study. Although there is room for further investigation on the simulation, we consider that the short period waves seen in the observed data can be explained by the site effect of the Sarobetsu basin.

4. CONCLUDING REMARKS

The spatial distribution map and attenuation relationship of the PGV (peak ground velocity) values from the 2003 Tokachi-oki earthquake (Mj 8.0) are controlled by the radiation pattern of long-period S and surface

waves, and various basin site effects. Especially long-period surface waves with periods of 10 to 30 s mainly contribute to the PGV values at distances larger than 200 km. We should note that the PGV attenuation relationship for the 2003 Tokachi-oki earthquake is derived from a specific station configuration in northern Japan, and it is not appropriate to apply this attenuation relationship to other large earthquakes occurring at different regions, as the general relationship.

ACKNOWLEDGEMENTS

We thank to Dr. H. Nagumo for providing his program code of the finite-difference method. K-NET, KiK-net and F-net strong-motion data were provided by National Research Institute for Earth Science and Disaster Prevention. The 95-type accelerometer data were provided by Japan Meteorological Agency. The centroid moment tensor solution was provided by Harvard University. Some of the figures in this paper were made using GMT (Wessel and Smith, 1995). This work was supported in part by the Grant-in-Aid for Scientific Research No. 16310120 from the Ministry of Education, Culture, Sports, Science and Technology, Japan.

REFERENCES

- Aoi, S. and H. Fujiwara (1999). 3D finite-difference method using discontinuous grids, *Bull. Seism. Soc. Am.* **89**, 918-930.
- Bouchon, M. (1981). A simple method to calculate Green's functions for elastic layered media, *Bull. Seism. Soc. Am.* **71**, 959-971.
- Hatayama, K., S. Zama, H. Nishi, M. Yamada, Y. Hirokawa and R. Inoue (2004). Long-period strong ground motion and damage to oil storage tanks due to the 2003 Tokachi-oki earthquake, *Zisin 2* **57**, 83-103 (in Japanese with English abstract).
- Kawase, H. (1993). Review: Amplification of seismic waves by sedimentary layers and its simulation, *Zisin 2* **46**, 171-190 (in Japanese with English abstract).
- Kawase, H. and T. Sato (1992). Simulation analysis of strong motions in Ashigara Valley considering one- and two-dimensional geological structures, *J. Phys. Earth* **40**, 27-56.
- Koketsu, K., K. Hatayama, T. Furumura, Y. Ikegami, and S. Akiyama (2005). Damaging long-period ground motions from the 2003 Mw8.3 Tokachi-oki, Japan earthquake, *Seism. Res. Lett.* **76**, 58-64.
- Maeda, T. and T. Sasatani (2004). Strong ground motions from the 2003 Tokachi-oki earthquake, *Geophys. Bull. Hokkaido Univ.* **67**, 167-179 (in Japanese).
- Maeda, T. and T. Sasatani (2006). Two-layer Qs structure of the slab near the southern Kurile trench, *Earth Planets Space* **58**, 543-553.
- Maeda, T. and T. Sasatani (2008). Long-period ground motions from the 2003 Tokachi-oki earthquake, *J. Seismol* **12**, 243-253.
- Morikawa, N., T. Kanno, A. Narita, H. Fujiwara and Y. Fukushima (2006). New additional correction terms for attenuation relations of peak amplitudes and response spectra corresponding to the anomalous seismic intensity in northeastern Japan, *Journal of JAEE* **6**, 23-41 (in Japanese).
- Suzuki, H., K. Iwamoto, M. Morino, H. Shinohara, H. Fujiwara, S. Aoi and Y. Hayakawa (2004). Modeling subsurface structure for seismic hazard map in Hokkaido area, *Proceeding of the 111th Society of Exploration Geophysicists Japan*, 49-52 (in Japanese).
- Takeo, M. (1985). Near-field synthetic seismograms taking into account the effects of anelasticity - the effects of anelastic attenuation on seismograms caused by a sedimentary layer -, *Meteorology and Geophysics* **36**, 235-257 (in Japanese with English abstract).
- Wessel, P. and W. H. Smith (1995). New version of the Generic Mapping Tools released, *EOS Trans. AGU*, 329.
- Yoshida, K. and T. Sasatani (2005). Long-period ground motion in the northwestern part of the Ishikari plain during the 2003 Tokachi-oki earthquake, *Zisin 2* **58**, 107-113 (in Japanese with English abstract).